JVST A
Journal of Vacuum Science & Technology A
ARTICLE
avs.scitation.org/journal/jva

Pattern dependent profile distortion during plasma etching of high aspect ratio features in SiO_2

Cite as: J. Vac. Sci. Technol. A **38**, 023001 (2020); doi: 10.1116/1.5132800
Submitted: 19 October 2019 · Accepted: 17 December 2019 ·
Published Online: 8 January 2020

View Online Export Citation CrossMark

Shuo Huang,[1,a)] Seungbo Shim,[2] Sang Ki Nam,[2] and Mark J. Kushner[1,b)]

AFFILIATIONS

[1]Department of Electrical Engineering and Computer Science, University of Michigan, 1301 Beal Ave., Ann Arbor, Michigan 48109-2122
[2]Samsung Electronics Co., Ltd., 129 Samsung-ro, Yeongtong-gu, Suwon-si, Gyeonggi-do 443-742, South Korea

Note: This paper is part of the Special Topic Collection Commemorating the Career of John Coburn.
[a)]**Present address:** KLA Corp., 2350 Green Road, Suite 100B, Ann Arbor, MI 48105; **electronic mail:** shuo.huang@kla.com
[b)]**Author to whom correspondence should be addressed:** mjkush@umich.edu

ABSTRACT

As aspect ratios of features in microelectronics fabrication increase to beyond 100, transferring patterns using plasma etching into underlying materials becomes more challenging due to undesirable feature distortion such as twisting, tilting, and surface roughening. These distortions can be attributed to several causes including the randomness of reactive fluxes into features, charging, and pattern dependencies. Randomness mainly results from disparities in the fluxes of etching species into adjacent features, which can be exacerbated when reaching the etch front in high aspect ratio (HAR) features due to conduction limits. These stochastic variations in energy, angle, and sequence of the incident species into adjacent features, rather than reactor scale nonuniformities, produce many of the feature-to-feature variations in etch performance. Pattern dependent distortion results from interference between the features due to charging of the feature surfaces. The resulting electric fields act not only on the ions incident into a given feature, but also on the ions in adjacent features. With symmetric patterns, stochastic charging of the inside surfaces of features results in tilting of HAR features in random directions. However, with nominally identical neighboring features, electrical forces on ions inside the features should, in principle, cancel. Statistical variations will produce some random tilting; but on average, there is no systematic tilting. With asymmetric patterns, horizontal electric fields are generated by feature charging that point from dense (more positively charged) to sparse (less positively charged) areas of the pattern. These net electric fields deviate ions from normal incidence and produce systematic tilting.

I. INTRODUCTION

In plasma etching for semiconductor fabrication, patterns are transferred from the overlying masks to underlying features, ideally replicating the mask pattern.[1,2] For achieving high selectivity in plasma etching, different mask materials are used such as photoresist (PR), amorphous carbon layers (ACLs), and organic planarization layers.[3] The principle of anisotropic plasma etching is that vertically directed ions onto the substrate will replicate the overlying patterns by activating etch processes on the horizontal bottom of the feature and not on the sidewalls. Due to the decrease in logic feature sizes, now sub-10 nm, and increase in aspect ratio (AR) for 3D NAND memory products, feature distortion is becoming more problematic. Feature distortion is the inability to transfer the desired pattern into the underlying material. Common distortions include twisting (a circular pattern does not produce a circular feature), tilting (the feature is etched at an angle instead of vertically), bowing (feature sidewalls are curved instead of straight), and edge roughening (inside surfaces of features are not smooth).

Distortions such as bowing are systematic—that is, the distortion appears consistently in all features. Systematic distortions such as bowing can usually be explained by ion fluxes into the feature that are angularly broad or having been reflected from other surfaces. The other distortions are typically statistical—that is, the severity of the distortion varies from feature to feature. These distortions are ascribed to several causes, including charging of the feature by ions and electrons from the plasma, polymer deposition, and pattern dependencies.[4–6] In some cases, sidewall roughening can originate from distortions in the pattern in the mask, which are transferred into the underlying materials.[6,7] These mask distortions may originate in the lithography or during the plasma process. With increases in AR to greater than 50–100, small distortions in, for example, tilting are magnified by the depth of the feature. The end result can be a decrease in the spacing between adjacent vias, even leading to bridging of adjacent vias.[8,9]

The density of a pattern of features refers to the number of features per unit area and is typically measured as the pitch of the pattern—the distance between the centers of adjacent features. With pitches of hundreds of nanometers to tens of nanometers, there is no systematic variation in the incident fluxes into adjacent features. With mean free paths of electrons, ions, and neutrals in the plasma greatly exceeding the pitch, there cannot be a significant gradient in reactant fluxes from the plasma incident into one feature and its neighboring features. In these cases, the dominant source of differences in fluxes into the adjacent features is simply the stochastic nature of the fluxes. The features are so small that the fluxes (magnitude and identity of reactants) into adjacent features have a significant stochastic component. This randomness can be magnified in high aspect ratio (HAR) features due to conduction limits and diffusive reflection at sidewalls for the etching species.[10,11] The time intervals between particles incident into the feature are usually much larger than the transit time of the particles in the feature, which makes the profiles sensitive to the sequence of the incident particles. Thus, small variations in energy, angle, and sequence of incident etching species in different features may cause feature-to-feature variations in etch performances (e.g., etch rate and selectivity).

Charging on the walls of a single feature during plasma etching produces internal electric fields that perturb the trajectories of anisotropic positive ions traversing the feature. Due to the differing angular distributions of electrons and positive ions, the tops of features typically charge negatively while the lower parts of the features charge positively. When etching nonconductive materials (e.g., SiO_2 and Si_3N_4), the electric fields produced by charge in a given feature can affect ion trajectories in neighboring features through the penetrating electrostatic fields.[12] In addition to the intrinsic randomness of charging of small features, the electrostatic interference from neighboring features is another source for profile distortion and feature-to-feature variation, which now depends on the adjacency, that is the pattern, of these neighboring features. With the pitch between features continuing to decrease, the electrostatic interference from adjacent features becomes more problematic.

Etching of patterns of HAR vias by plasmas sustained in fluorocarbon/oxygen gas mixtures was experimentally investigated for via diameters of 50–200 nm and ARs of 10–30.[13] Statistical variations in profiles, etch rates, and pattern distortion were observed from feature to feature. By using a cyclic process of alternating etching and deposition phases for SiO_2 processing, bowing at low ARs (∼5) and feature-to-feature variations in critical dimensions (CDs) at high ARs (>20) were both reduced.[14] The anisotropy of the profiles was improved due to polymer deposition on the sidewalls during the deposition phase. The polymer deposited at the interface between the mask and the oxide significantly affected the degree of pattern distortion, which could be alleviated by adding an *in situ* polymer removal step during the over-etch.[7–15] (For brevity, the term *oxide* refers to silicon dioxide, SiO_2, and *nitride* refers to silicon nitride, Si_3N_4.) Defects in the mask produced by erosion during the etching process can be transferred to the sidewalls of HAR features.[6] Suppressing mask degradation was found to decrease feature distortion and alleviate twisting at high ARs when transferring patterns in ACL into SiO_2 with different pitch sizes.

Feature-to-feature variations become more severe when etching hybrid materials such as alternately deposited oxide-silicon-oxide (O–Si–O) and oxide-nitride-oxide (O–N–O) stacks. In the plasma etching of channel holes in O-Si-O stacks using HBr/fluorocarbon mixtures, the sidewall of the features changed from smooth to scalloped when the HBr fraction was increased.[16] Surface adsorption of N–H and Br was enhanced resulting in reduced polymer thickness and enhanced Si etching. In the modeling and characterization of feature distortion during plasma etching of source/drain contacts, the consequences of random variation in the mask on distortion outweighed systematic variations when the CD decreased below 32 nm.[17,18] A voxel-slab model was used to investigate contact hole etching in SiO_2, showing that profile distortion due to physical damage in the SiO_2 was reduced by maintaining a critical thickness of the overlaying polymer.[19,20] Results from a three-dimensional Monte Carlo model indicated that ion induced surface roughness can be mediated by the use of etch inhibitors.[21]

In this paper, results are discussed from a computational investigation of feature distortion during plasma etching of HAR vias in SiO_2 using trifrequency capacitively coupled plasmas (TF-CCPs) sustained in $Ar/C_4F_8/O_2$ mixtures. The fluxes of ions and neutrals and ion energy and angular distributions (IEADs) were obtained from reactor scale modeling performed using the Hybrid Plasma Equipment Model (HPEM). The feature scale modeling was performed using the three-dimensional Monte Carlo Feature Profile Model (MCFPM). Feature-to-feature variations in the shape of the vias mainly result from randomness in the fluxes of particles into the features rather than reactor scale nonuniformities. The charging of features in symmetric patterns results in features tilting in random directions. With asymmetric patterns, charging produces tilting toward open areas of the pattern due to horizontal components of the E-field induced by the laterally asymmetric charging. The tilting can be alleviated to some degree by increasing the bias power, which increases the ion energy and decreases the etch time, resulting in less deviation in ion trajectories by these lateral electric fields.

Descriptions of the models used in this investigation are in Sec. II. Results from the study for the etching of multiple vias in different patterns are in Sec. III. Concluding remarks are in Sec. IV.

II. DESCRIPTION OF THE MODELS

Integrated reactor and feature scale models were used to investigate plasma etching of multiple HAR vias in SiO_2 using TF-CCPs. The fluxes of ions and radicals to the wafer and the IEADs were obtained from the reactor scale modeling using the HPEM (Ref. 22), which is discussed in detail in Ref. 23. An $Ar/C_4F_8/O_2$ gas mixture was used. The species and gas phase reactions included in the reaction mechanism are the same as in

Ref. 23. The resulting profile evolution and etch properties were obtained by feature scale modeling with the MCFPM.[11,24]

The MCFPM is a three-dimensional voxel-based model utilizing a cubic-mesh. Briefly, each cell in the numerical mesh may represent a different solid material. Gas phase pseudoparticles are launched with their initial velocities sampled from the IEADs obtained from the HPEM. Pseudoparticles striking surfaces can sputter, activate chemical reactions, deposit, implant, and reflect, thereby changing the identity of the underlying mesh cell or adding a solid mesh cell. Energetic pseudoparticles can penetrate beneath the surface to activate subsurface chemical reactions. Charged species striking solid surfaces deposit charge, which produces charge densities used in solving Poisson's equation for the electric potential. The resulting electric fields are then used to advance the trajectories of charged particles passing through the feature. In this investigation, the mask, SiO_2, and fluorocarbon polymer deposits have essentially no electrical conductivity, and so the electric fields produced by charge inside one feature can penetrate into adjacent features.

The reaction mechanism used in the MCFPM for predicting profile evolution in SiO_2 by $Ar/C_4F_8/O_2$ plasmas is described in Ref. 23. Briefly, the pristine SiO_2 surface is activated by energetic species (ions and hot neutrals). The activated surface has higher reactivity for passivation by polymerizing C_xF_y radicals. Further deposition of C_xF_y species on the passivated surface forms polymers, whose thickness can be controlled through etching by atomic oxygen species produced by the dissociation of the O_2. The energetic species reaching the passivated surface ($SiO_2C_xF_y$) remove the oxide in the form of volatile SiF_x and CO_x, which is the process of chemically enhanced etching (i.e., chemical sputtering). The SiO_2 can also be directly removed from the surface through bombardment by energetic species through physical sputtering, which requires higher threshold energies than chemical sputtering.

III. ETCHING OF MULTIPLE VIAS IN PATTERNS

The geometries and initial patterns of PR for etching multiple HAR vias are shown in Fig. 1. Two symmetric patterns of four vias were investigated: a linear array and a 2×2 square pattern. The asymmetric patterns investigated were a four via off-axis arrangement and linear arrays with one via missing. Gas phase particles leaving the sides of the computational domain were reflected back into the domain, reflective boundary conditions, while gas phase particles leaving the top of the domain were removed from the simulation. Reflective boundary conditions were also used for mesh properties across the lateral boundaries of the pattern, including material identities and charge. With periodic boundary conditions, the unit pattern shown in Fig. 1 can represent full-pitch (for the linear array and square unit) and half-pitch patterns (for off-axis unit).

The distance between the centers of the adjacent vias was 100 nm and the diameters of the holes in the PR mask were 50 nm. The thickness of the SiO_2 was 2000 nm, with 670 nm thick PR as the mask and Si as the stopping layer. The total aspect ratio for perfect pattern transfer from the top of a pristine mask to the stop layer is 53. The AR of only the SiO_2 is 40. Unless otherwise noted, the AR in the following discussion refers to the depth of the etched feature in the SiO_2. The meshes consist of $40 \times 160 \times 1084$ cells for the linear pattern, $59 \times 146 \times 1084$ for the off-axis pattern, and

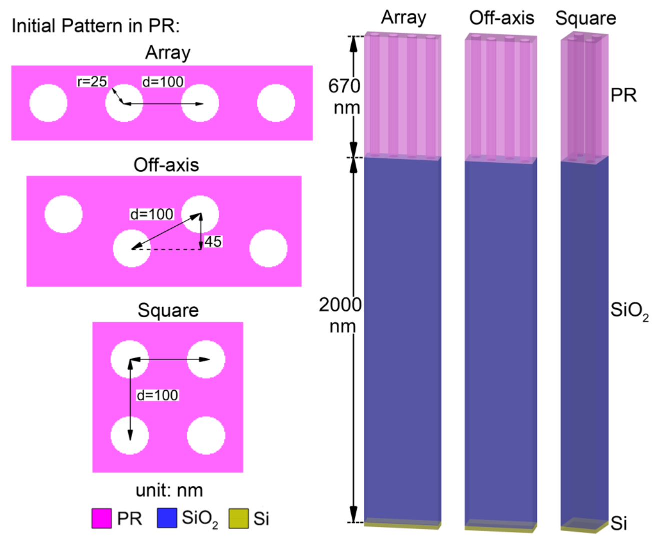

FIG. 1. Schematic of the patterns (linear array, off-axis, and square) in the photoresist and the geometries of the initial profiles. The height of the SiO_2 is 2000 nm with 670 nm thick photoresist as the mask and Si as the stopping layer.

$80 \times 80 \times 1084$ for the square pattern, producing cubic voxels of 2.5 nm on a side. The dielectric constants (ϵ/ϵ_0) of the materials used in the solution of Poisson's equation were as follows: SiO_2, 4.0; photoresist, 3.0; and polymer, 3.0.

The fluxes of the ions and radicals and IEADs were obtained from the reactor scale modeling of a TF-CCP sustained in $Ar/C_4F_8/O_2$ mixtures. The role of Ar in the mixture is primarily to provide energetic, chemically inactive, Ar^+ ions onto the surface for physical activation of processes. C_4F_8 is dissociated by electron impact to produce polymerizing CF_x and C_xF_y species, which deposit on the surface of the oxide and serve as the fuel to remove silicon and oxygen sites while protecting the sidewalls. O_2 is dissociated to produce O atoms that are used to control the amount of polymer deposition at the surface to avoid clogging while allowing etching species (e.g., ions and neutral radicals) to reach deeper into features.

Three frequencies (80/10/5 MHz) were used to provide a large dynamic range for tuning the plasma properties and the IEADs. The 80 MHz power applied on the top electrode was mainly used as the source power for sustaining the plasma. The 10 and 5 MHz powers applied on the bottom substrate were mainly used to accelerate the ions to the surface with customized IEADs. For the base case, the powers of the three frequency sources (80/10/5 MHz) were 400/2500/5000 W. The corresponding voltages to deliver these powers were 125/1030/2450 V, with a dc bias of −1690 V. The ions have high energy (1400–3000 eV) and narrow incident angles (less than 3°), which are desirable for HAR etching by reducing sidewall impacts and producing anisotropic profiles.

Charging of the surfaces on the top and inside of the feature occurs in dielectric etching or in conductor etching using polymerizing gas mixtures. As described above, positive ion pseudoparticles are launched toward the surface with velocities sampled from the

IEADs obtained from the HPEM. (Essentially no negative ions reach the surface.) A corresponding flux of electron pseudoparticles is launched toward the surface to provide a charge neutral flux. The velocities of the electrons are randomly chosen from an isotropic Maxwellian distribution having a temperature of 4 eV. Due to the computational expense of solving Poisson's equation, the electric potential is updated only after 400 charged particles strike the surface. During the execution of the MCFPM, millions of charged particles are launched. The resulting profiles do not significantly change when increasing the rate of solving Poisson's equation. The bottom of the computational domain is electrically grounded. Since the actual thickness of the wafer is not resolved in the MCFPM, three thin dielectric layers were added between the stopping layer and the ground plane. The dielectric constants of these layers were adjusted so that the capacitance of the feature with respect to the ground plane is the same as for the actual thickness of the wafer.

A. Statistical feature-to-feature distortion with symmetric patterns

Sectional views during plasma etching cleaved through the center of the linear array as a function of time are shown in Fig. 2. The time between each frame is the same, except for the first frame showing the profile at the very beginning of etching. When examining individual vias, the general trend of profile evolution is quite similar to that of etching a single HAR via, as discussed in Ref. 23. Key features are captured including eroded PR mask, bowing in the upper portion of the features at AR of 5 and a tapered etch front. Due dominantly to ion sputtering, the PR is eroded during plasma etching, resulting in a SiO_2-to-PR selectivity of 10. This erosion leads to roughness on the top, beveled surfaces, and sidewalls of the PR.

As the etching proceeds, the etch front of each via propagates downward (normal to the surface), without major tilting or twisting. As the pitch of the pattern is 100 nm, there is no systematic change in the incident fluxes across the array. That is, there is no systematic variation in any reactor scale plasma properties across the dimension of the array. The randomness in the shape of vias and etch rates result from the stochastic nature of the fluxes of radicals and ions incident into adjacent features. Although there is variation in the etch rate of as much as 10% due to the stochastic arrival of reactants, by having an over-etch period, the side-by-side features do eventually bottom-out on the stopping layer in a fairly uniform manner.

With the diameter of the hole in PR being 50 nm and fluxes incident into the hole being about $10^{15}\,cm^{-2}\,s^{-1}$ for ions and $10^{17}\,cm^{-2}\,s^{-1}$ for neutral radicals, the ions and radicals arrive into the feature with time intervals of 10^{-5} and 10^{-7} s, respectively. For ion and hot neutral energies in excess of 1000 eV and the thermal neutrals of 0.03 eV, the transit time through the feature or the residence time within the feature before leaving is about 10^{-10} s (for ions and hot neutrals) and 10^{-8} s (for thermal neutrals). Having said that, there may be tens to hundreds of reflections of thermal neutral particles within the feature before exiting. These reflections could extend the residence time to as long as 10^{-6} s. Even for these long times, the likelihood of having multiple particles in the feature (or having particles interact in the feature) is small.

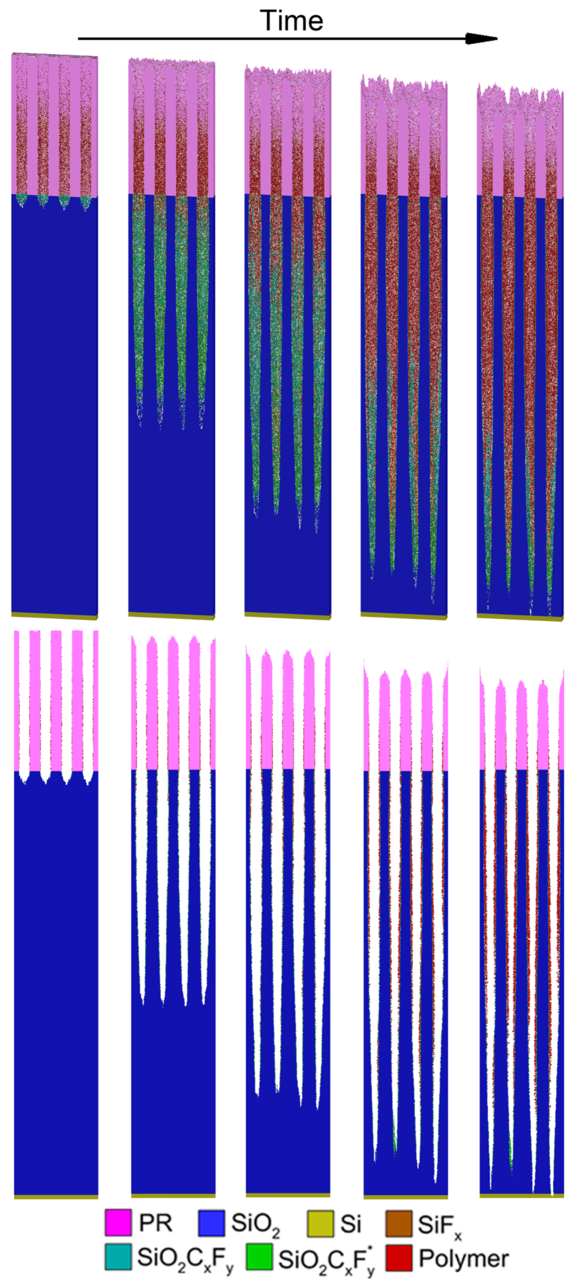

FIG. 2. Section view (top) and central slice (bottom) of profile evolution during etching of HAR features in a pattern of four linear vias. The first frame is at the beginning of the etching, while the other four frames are sampled with the same time interval.

The statistical variation in fluxes results in adjacent features receiving different mole fractions of species having different sequences of arrival, and different energies and angles of each individual species. These differences produce feature-to-feature variations in etch properties. These differences generally cannot be rectified or averaged out without increasing the number of particles arriving in the feature by increasing the magnitude of fluxes. Due to the finite angular spread of ions, nonspecular reflection of energetic particles, and gas conduction limits, the fluxes of energetic particles (ions and hot neutrals) and radicals decrease by factors of 10 and 50, respectively, as the AR of the via increases from 0 to 40. This decrease in fluxes increases the randomness and stochastic variation in the etching species reaching the etch front. The MCFPM uses pseudoparticles that individually represent hundreds of atoms. This weighting exaggerates these stochastic effects in sampling the pseudoparticles from the total fluxes as well as sampling the energy and angle of the ions from the IEADs.

As the AR increases during etching, the feature-to-feature variation becomes reinforced, rather than being attenuated, due to there being fewer ions and radicals reaching deeper into features that are then more subject to randomness. Although there is no systematic tilting, individually features do tilt in random directions. The tilting has many origins. A statistically thicker layer of polymer on one side of the feature will produce a different angular distribution of specularly or diffusively reflected ions, which may preferentially etch the opposite wall. (Here, the term ion refers to both the incident charged particle and the hot neutral produced when the ion first strikes a sidewall.) Statically, more positive charge on one side of the feature, which may be trapped in polymer, will perturb ion trajectories toward the opposite side of the feature. Once tilting develops at low ARs, the tilting will be enhanced and transferred deeper into the feature, rather than being rectified or reversed unless the physical origin of the asymmetric trajectories in the feature is changed. That is, if positive charge is asymmetrically trapped in polymer on the sidewall, all subsequent ion trajectories will be perturbed until that trapped charge is removed or neutralized. Taking the linear array pattern as an example, the second feature from the right slightly tilts rightward while the first feature from the right slightly tilts leftward starting from an AR of 20, as shown in Fig. 2. As the AR increases to 40, the tilting directions of these two features are maintained. The end result is that their etch fronts approach each other to a distance of 90 nm, which is smaller than the pitch in the PR pattern by 10 nm (10% loss in pitch).

The charge densities deposited at the top and inner surfaces of the features, and the electrostatic potentials produced by these charges, are shown in Fig. 3 for the same time intervals as in Fig. 2. The electrons predominantly deposit charge on the top surfaces, beveled surfaces, and the shallow sidewalls of the PR, reaching a maximum of $-46.4\ \mathrm{C/cm^3}$ on the beveled surface of the PR. Positive ions reach more deeply into features due to their anisotropic IEADs. The positive ions deposit their charge on the surface and reflect as hot neutrals. For small AR, the ions initially strike the bottom of the feature, and this is the location of the maximum in positive electric potential. With increasing AR, ions (having a finite angular spread) will eventually strike the sidewall and deposit charge on the sidewall. Beginning with an AR of about 15, the electric potential has its maximum potential on the sidewalls at this depth. An electric field is established pointing from the middle of the feature upward toward the top of the feature, and downward into the feature. A near quasisteady state is established wherein the rate of charging of the feature by positive ions is balanced by

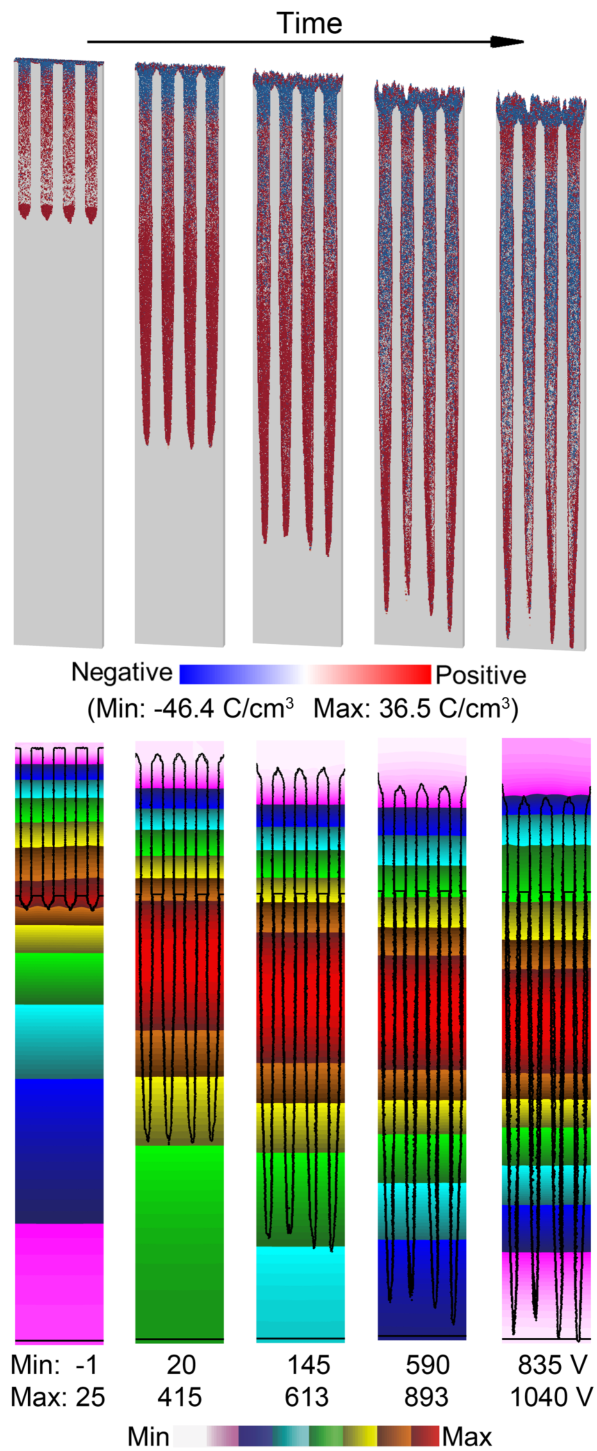

FIG. 3. Time evolution of charge distribution (top, section view) and electric potential (bottom, central slice) during etching of HAR features in a pattern of four linear vias. With reflecting boundary conditions, the pattern is symmetric. The frames are sampled at the same time as in Fig. 2.

electrons attracted into the feature by the upward pointing electric field.

Ions incident into the feature with a small angle and energy greater than the maximum in electrostatic potential will decelerate and then accelerate when approaching and passing the maximum in potential. The ions will reach deeper into the feature with a decrease in their energy determined only by the local electric potential and not the maximum in electric potential. This is a fundamentally different situation than when the maximum in electric potential is on the bottom of the features. Ions that neutralize by striking the sidewall above the maximum in electrostatic potential produce hot neutrals that proceed deeper into the feature unaffected by the electric fields. In large part, ions whose trajectories are perturbed by these in-feature electric fields to produce tilting are those ions that either pass by or neutralize near the maximum in electric potential.

Due to the stochastic variations in the number, sequence, energy, and angle of the incident particles into the features, the profiles in Fig. 2 have a maximum of 7% difference in etch rate and 5% difference in the bowing CDs. One solution for mitigating the feature-to-feature variation in the etch rate and CD at the bottom of the feature is to allow for some significant over-etch time to ensure that all the features are etched through and the bottom CDs are wide enough for the subsequent process step. The surfaces of the final etch profiles with 10% over-etch are shown in Fig. 4 for different patterns. By allowing for 10% over-etch, the etch fronts all reach the stopping layer with at least a 20 nm hole opening at the bottom. The bowing CDs vary from feature to feature by less than 5%, with the maximum bowing CD being 72 nm. Overall, the statistical disparities in feature profiles can be diminished by allowing for over-etch, which increases the total fluence of particles into the feature.

In radio frequency (RF) excited plasmas, ions are accelerated toward the surface by the electric field in the sheath resulting in a nearly continuous flux onto the surface. Electrons reach the surface dominantly during the anodic portion of the RF cycle. After initial negative charging of the surface to produce the floating potential, equal fluxes of electrons and ions averaged over the RF cycle result in a charge neutral flux to flat surfaces. Patterned surfaces with HAR features enhance or restrict the relative fluxes of electrons and ions to surface inside the features due to the difference in the angular distributions of the electrons and ions. The end result is a spatial variation of the charge distribution and thus electric potential along the inner sidewalls of the features in SiO_2. A linear array with reflective boundary conditions is equivalent to having an identical mirror image of the array across the boundary or features with a constant pitch in every direction. With the resulting symmetric charge distribution, the electric potential at a given height is quite uniform, as shown in Fig. 3. Any feature-to-feature variation in electric potential is due to statistic variation in charging and is systematic. The symmetric charge distribution produces electric fields that act on adjacent features from both sides, producing no net electric fields that would systematically deflect ion trajectories. There may be some random interference between features, but no systematic interference.

Ideally, the initially circular mask opening in the PR should be faithfully transferred to the feature during plasma processing. Due

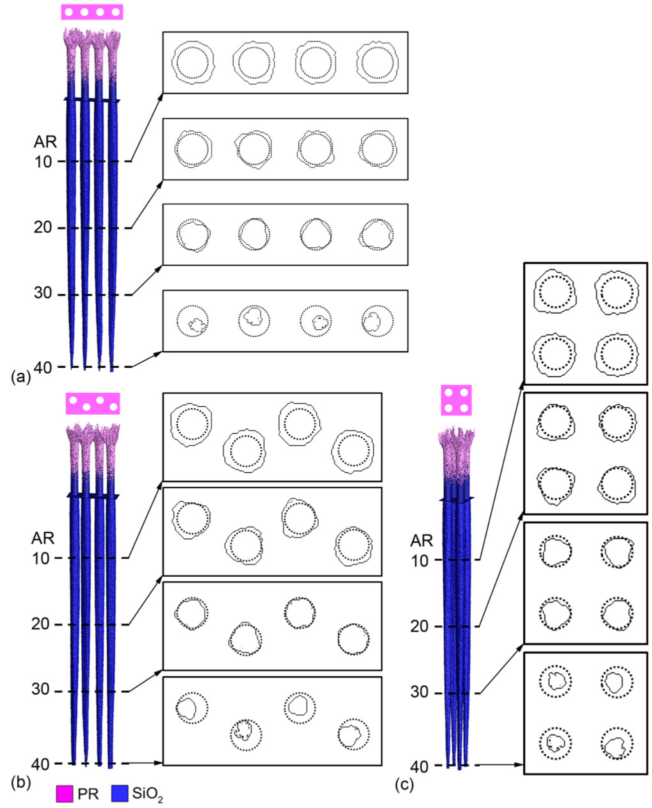

FIG. 4. Horizontal slices through multiple vias showing the edge of the SiO_2 surface for aspect ratios of 10, 20, 30, and 40 after a 10% over-etch. (a) Liner array, (b) off-axis, and (c) square patterns. The dotted circles are projections of the initial hole in the PR mask.

to nonuniformities in mask materials and stochastic processes during plasma etching, feature distortion such as contact edge roughness (CER), line edge roughness, or elliptical profiles can develop.[7,25,26] Profiles through square and linear symmetric patterns after a 10% over-etch are shown in Fig. 4. These profiles are shown with the polymer removed indicating the shape of the profiles that would result after a perfect cleaning process. The initial mask opening is shown by the dotted circles. Profile outlines wider than the opening indicate bowing, which is most severe at AR = 5–10. Profile outlines narrower than the mask opening indicate tapering. Profile outlines that are noncircular indicate distortion. If the centroid of the profile is not at the center of the circle, then the feature has tilted.

The horizontal sections shown in Fig. 4 are close to circular, though with some bowing, for ARs < 20. For larger AR, the profiles begin to distort. With AR > 30, the profiles have smaller diameters (<50 nm) and more anomalies due to tapering of the etch front. The distortion is due to the stochastic nature of the reactants entering the feature and is worse deeper in the feature that receives less flux due to conduction limits and hot neutrals having less energy than the original ions. Locations deeper in the feature also experience less local over-etch that tends to round-out the feature. Distortion is in large degree statistical. With symmetric patterns, there is some random tilting due to random surface charging in both the feature and adjacent features. However, this tilting is not systematic—that is, there is not an array wide trend in tilting.

As the etching proceeds, the PR is eroded dominantly by ion sputtering, resulting in the PR having rough beveled and top surfaces as shown in Fig. 2. The features at the PR level become less distinct as the beveled surfaces of adjacent holes intersect those of their neighbors. If the PR erodes to the extent that the beveled surfaces reach the SiO_2 interface, scattering of the ions from the roughened beveled surfaces into the feature will enhance bowing, a situation that does not occur here due to the large initial height of the PR. The roughening of the PR will produce some channeling of grazing ions scattering from the inner surface of the PR that can be a source of CER in the SiO_2. For these conditions, little CER was observed from this source. The major effect of the roughness of the PR was diffusive scattering of grazing ions, which contributes to the edge roughening and bowing by having more normal incident ions.

The CER mainly originates from the randomness in the energetic ions and polymerizing radicals into the features. Due to the small number of ions into the feature, the activation energy provided by the ions will not be uniformly distributed along the circumference of the feature at all ARs during the whole processing time. Nonuniform polymer deposition on the sidewalls adds to the roughness produced by ions by providing sites for diffusive scattering and nonuniform passivation of SiO_2. This effect is exacerbated at high AR (>30) where surface coverage by polymer is spotty due to conduction limits for transport of polymerizing radicals deep into the feature and redeposition of etch products. The distortion tends to be self-perpetuating as once the feature becomes noncircular, specular ion scattering from the sidewalls is channeled to lower in the feature to replicate the same topology. This is again exacerbated at high AR where polymer coverage is less due to conduction limits. With sufficient polymer flux, dents and grooves in the sidewalls tend to be filled in by the polymer.

The deposition of polymer on the sidewalls for AR < 10 has a thickness of about 10 nm. This is in part due to the slowing of ions by the positive charging deeper in the feature, which reduces the rates of polymer sputtering and provides additional polymerizing radicals due to neutralization of slower CF_x^+ and $C_xF_y^+$ ions. The thicker polymer effectively increases the AR of the feature from 40 to closer to 50 by narrowing the open area. The larger effective AR then reduces fluxes deeper into the feature by worsening the conduction limited transport. The sidewall passivation is itself somewhat stochastic. All of these effects work against transport of neutral radicals deeper into the feature and work against specular reflection of ions from the sidewalls. The edge profiles at AR = 40 are then anomalous with small openings (less than 30 nm) even after 10% over-etch.

The horizontal slices at an AR of 40 are shown in Fig. 5 for the linear array after 10% over-etch with and without charging. (The effects of charging can be partly mitigated by fluxes of high energy electrons into the feature[4] or the use of pulsed power.[27]) The edge profiles shown in Fig. 5(a) for the noncharging case have larger hole openings (~50 nm), similar to the initial hole opening in PR. As the etch rate without charging is about 20% higher than with charging due to ions not being decelerated by the electric potential in the feature, a 10% over-etch results in more opening of the SiO_2 after reaching the Si stopping layer.

The profiles shown in Fig. 5(b) with charging are for different values of the random number generator seed in the simulation. A sequence of pseudorandom numbers is used to choose fluxes, scattering angles, and surface reactions during the simulations. Using a different random seed has the effect of sampling different parts of the die with statistically different incident fluxes while having the same time averaged values. The centroids of the profiles at AR = 40 for 10 cases with different random number seeds are shown in Fig. 5(c). The profiles with charging are more distorted and more-stochastic than in the absence of charging. The centroid of the feature for any given case will likely land somewhere other than

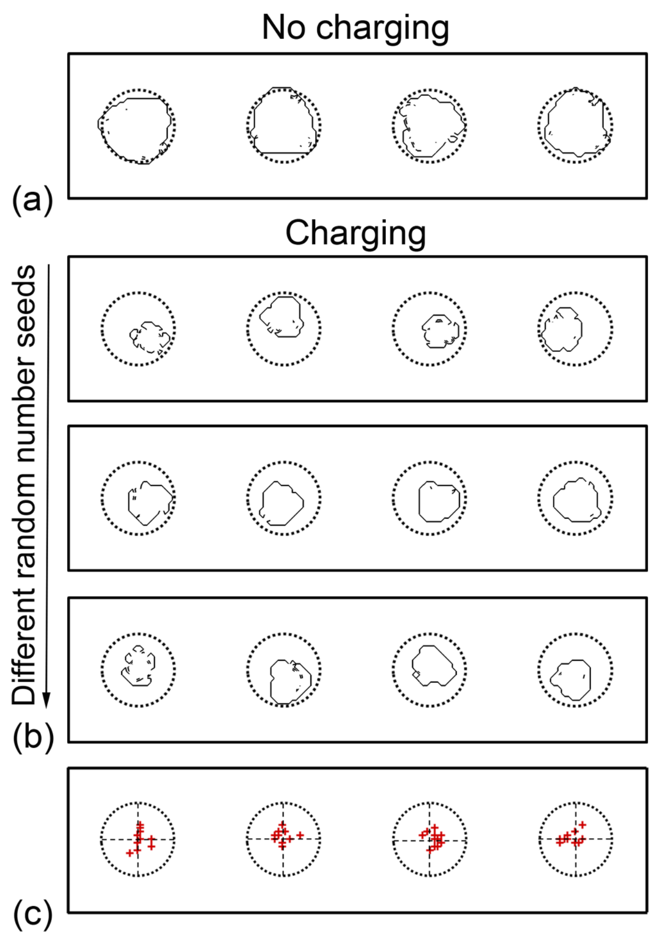

FIG. 5. Horizontal slices at the bottom of the SiO_2 (AR = 40) for final etch profiles with 10% over-etch for a symmetric linear array pattern. (a) Without charging, (b) with charging for different random number seeds in the simulation, and (c) statistics of the centers (denoted by "+") of the profiles at AR = 40 for 10 cases with charging. The dotted circles are projections of the initial hole in the PR mask.

directly under the center of the hole in the PR. That is, individual features do have random tilting, deflecting the center of the bottom of the feature by 10–20 nm. However, when averaged over many features, centroids of the individual features cluster around the center of the hole. That is, there is no systematic distortion or tilting of the features.

B. Feature properties with asymmetric patterns

Asymmetric pattern of features occurs at the edge of a die or when features with different sizes and shapes (e.g., circular, L-shape, and U-shape) are adjacent and simultaneously etched.[13] Imperfections in the lithography process can produce nonuniform patterning, which leads to local asymmetries within a large matrix of vias.[19,28] In this investigation, we investigate deliberately asymmetric patterns by removing one feature in the linear array.

The final etch profiles with 10% over-etch and horizontal slices at different ARs for the asymmetric linear pattern are shown in Fig. 6(a). The final profiles for AR = 40 for several cases with different random number seeds and the location of their centroids are shown in Fig. 7 as the 5 kW case. The fluxes and IEADs used here are the same as the base case with the symmetric pattern. Instead of random tilting of the features as with the symmetric patterns in Fig. 4, the features in the asymmetric pattern preferentially tilt in the direction of the missing via or toward open areas or less dense portions of the pattern. The tilting angles of the features adjacent to the missing via are larger than the more distant features. The collection of centroids of 10 cases [Fig. 7(b)] indicate that tilting for the asymmetric pattern has a systematic distortion.

The systematic tilting with the missing via results from the pattern level asymmetry in the charge distribution. As shown in Fig. 3, a positive electric potential is produced inside features. An electric field points radially outward from positive charged. Although there is statistical variation in the charging in each feature, on the average, the maximum electric potential occurs at about the same height. As a result, the electric field in a symmetric pattern from one feature is balanced by an oppositely pointing electric field from an adjacent feature. The end result is little lateral deflection of ions.

With an asymmetric pattern, the electric fields pointing away from the feature at the edge of a pattern is not balanced by an opposing electric field. This leaves a net electric field pointing from the dense to the less dense portions of the pattern. The direction of the electric field generally points up or down from the maximum in electric potential, as shown in Fig. 6(b). The upward pointing vertical component of the electric field is responsible for slowing ions approaching the maximum in potential. The downward pointing vertical component of the electric field is responsible for accelerating ions that are able to pass by the maximum in potential. Meanwhile, in the lateral (horizontal) direction, there is a net electric field component pointing toward the less dense pattern. The skewing of the electric field toward the less dense pattern is most severe at an AR of 11 where the horizontal electric field reaches a maximum of 4.5×10^5 V/cm. The trajectories of the incident ions are deviated by this horizontal electric field, resulting in tilting of the features in the same direction. An extreme case of producing electric fields pointing from dense to less dense patterns would be vias at the edge of the die bordering open field. Due to the smaller total amount of charge deposited in the asymmetric array, the maximum electric potential is 810 V, smaller by 22% than that for the symmetric array.

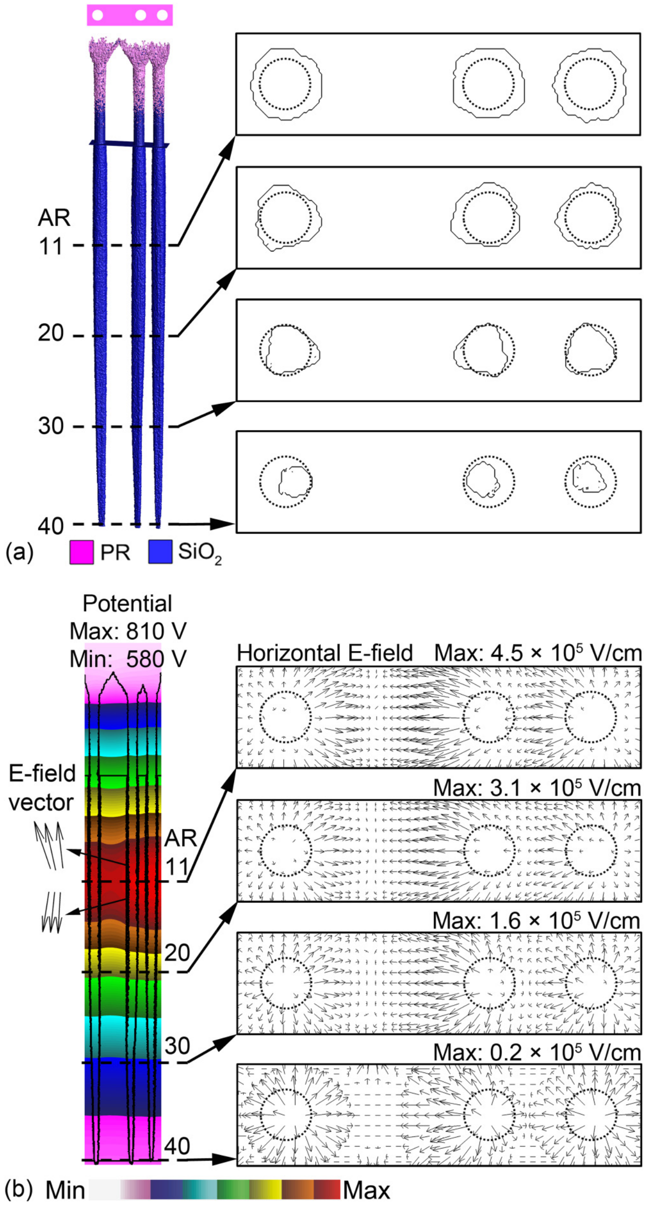

FIG. 6. Horizontal slices through an asymmetric pattern (1 via removed from the linear array) with 10% over-etch for ARs of 11, 20, 30, and 40. (a) Full feature and profile showing the outline of the SiO_2. (b) Electric potential for all features (central slice) and electric field vectors in the horizontal plane. The maximum electric potential occurs at AR = 11 where the direction of the total electric field is shown. The electric field vectors for each AR are separately normalized with the maximum electric field noted in the figure.

The asymmetric pattern with a missing via also produces nonuniform PR isolation between the vias. The right two vias in Fig. 6

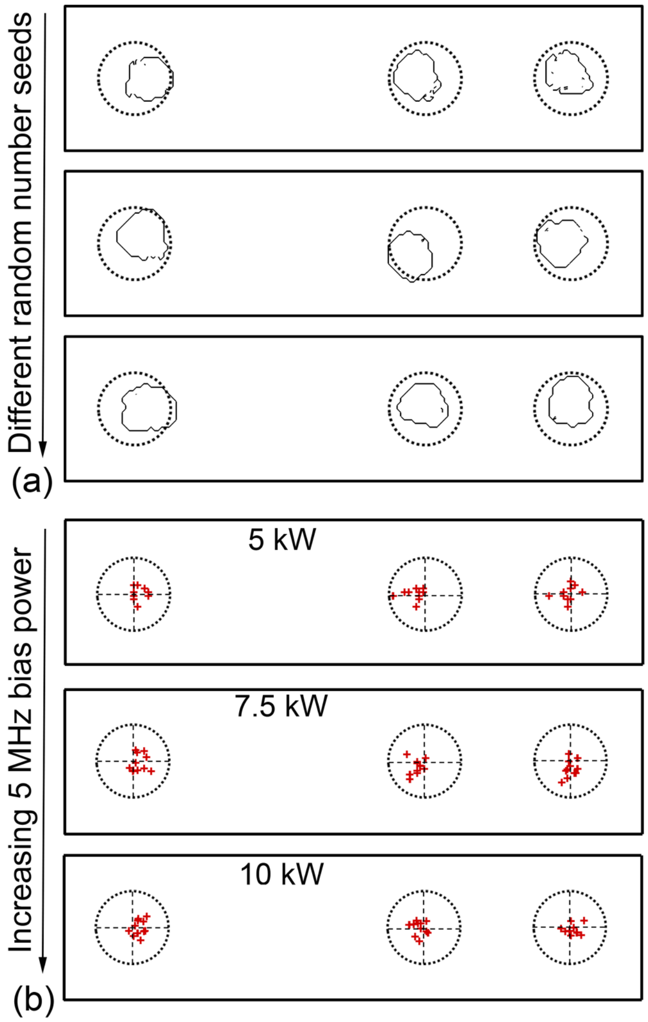

FIG. 7. Horizontal slices at the bottom of the SiO_2 (AR = 40) for final profiles with 10% over-etch for the asymmetric linear pattern (1 via removed). (a) With charging while changing the random number seed in the simulation. (b) Statistics of the centers (denoted by "+") of the profiles at AR = 40 for 10 cases with charging for different 5 MHz powers. The dotted circles are projections of the initial hole in the PR mask.

are isolated by PR having 50 nm thickness while the left two vias are isolated by PR having 150 nm thickness. This difference results in more height loss for the thinner PR than the thicker PR by about 80 nm. In this study, the PR retains a height of more than 400 nm at the end of the process. As a result, the difference in PR height loss due to the pattern asymmetry has little effect on the feature profiles in the oxide. However, for shorter PR mask heights that allow reflections from the PR bevels into the feature, the differential PR height loss may be a source of difference in etch properties and profiles for adjacent vias in a pattern.

The horizontal profiles at an AR of 40 for asymmetric patterns with different random number seeds are shown in Fig. 7(a) for a 5 MHz power of 5 kW. The centroids of ten profiles with different random number seeds for 5 MHz powers from 5 kW to 10 kW are shown in Fig. 7(b). In addition to statistical variation caused by the randomness of fluxes, the features have systematic distortion in the form of tilting from dense to less dense parts of the pattern. In this case, the tilting is toward the open space of the missing via. The tilting distortion is most severe for the vias adjacent to the open area, while less severe for the vias more distant from the open area. The horizontal profiles for the off-axis array shown in Fig. 4(b) shows some evidence of tilting toward the open area, though the effect is less weak as there is "open area" on multiple sides of vias.

With an increase in 5 MHz power from 5 kW to 10 kW, the average ion energy increases from 1900 to 2500 eV and the flux of ions increases from 0.9×10^{16} to 1.2×10^{16} cm^{-2} s^{-1}. The combination of higher energy ions having larger fluxes results in an increase in the etch rate by about 55%, which also reduces the time required for a 10% over-etch. The lower fluence of charged particles that the features are exposed to results in the maximum positive electrical potential in the feature decreasing from 810 V (5 kW) to 750 V (10 kW), about a 7% decrease, while ion energies, on the average, are higher (by about 30%). There is qualitatively a decrease in systematic tilting with higher bias over this range of powers, though the distortion is not eliminated.

C. Sparse and dense patterns

The pitch between features is generally decreasing in concert with the decrease in feature size.[28,29] For example, the HAR features in 3D NAND memory have less than 100 nm pitch. The distortion of features is generally more severe for smaller pitch.[6] The arrangement of features may be nonrectilinear (e.g., honeycomb patterns) to increase feature density while also optimizing isolation.[7,30] To investigate the dependence of feature distortion on pitch, HAR etching of symmetric patterns was simulated for layouts ranging from dense (pitch 80 nm) to sparse (pitch of 200 nm). These patterns were created by applying reflective boundary conditions on all boundaries of a cell having the pitch width. The diameter of the hole in PR is 50 nm for all patterns. Following a 10% over-etch, the centroids of the profile at the bottom of the feature (AR = 40) at the Si stop layer were recorded for 10–20 cases having different random number seeds. The locations of centroids are shown for 100, 150, and 200 nm pitches as in Fig. 8(a). The average displacements of the centroids and standard deviations are shown in Fig. 8(b).

The net positive charge accumulating in any single feature for the same incident fluxes is generally the same. However, the closer proximity of features for dense patterns results in the electrical potential being larger than in the sparse patterns. For example, the maximum in feature electrical potential for the 100 nm pitch was ≈1000 V while that for the 200 nm pitch was ≈300 V. The resulting decrease in energy for ions penetrating deeply into features with the dense 100 nm pattern decreases the etch rate by 40% compared to the sparse 200 nm pattern. With the closer proximity of the statistical charging in neighboring features with the dense pattern, the perturbing electric fields from neighboring features are larger. The resulting perturbation in ion trajectories then produces more statistical variation in the location that the feature lands on the stopping

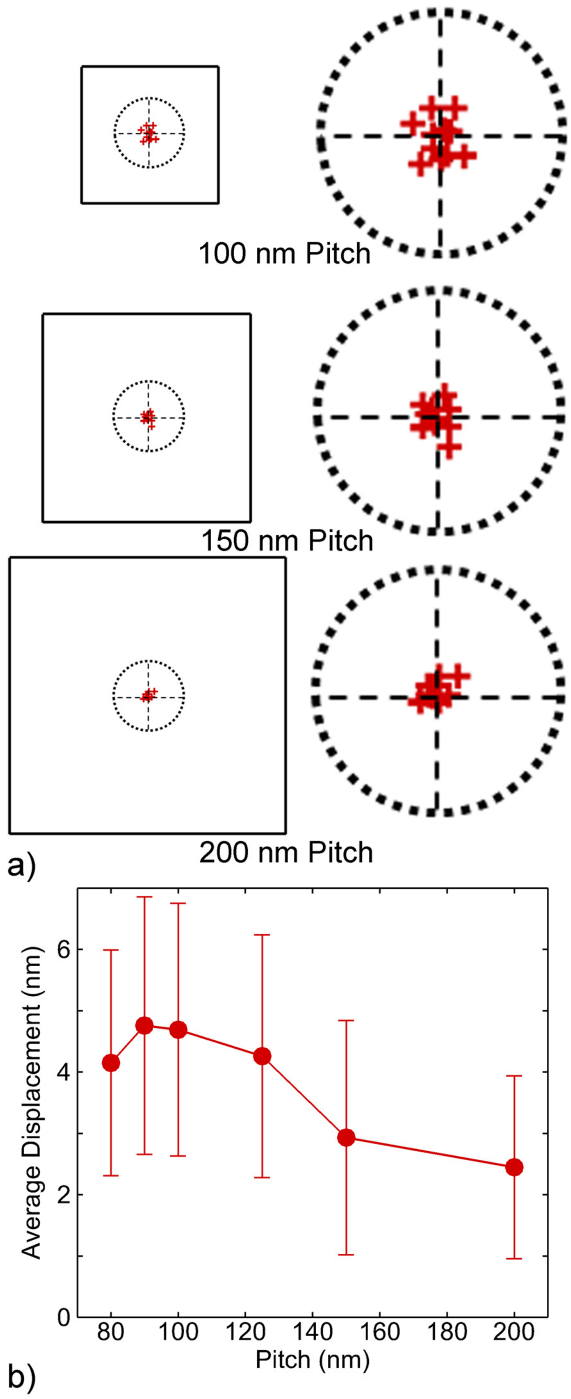

FIG. 8. Statistics of the centroids of the profiles at AR = 40 for 10–20 cases while varying the pitch of symmetric patterns. (a) Location of the centroids (denoted by "+") for pitches of 100, 150, and 200 nm. The dotted circles are projections of the initial hole in the PR mask. (b) Average displacement (with standard deviation error bars) of the centroids of the profiles from the center of the mask as a function of pitch.

later. The centroids of features with patterns below 100 nm vary by as much as 10 nm compared to only a few nanometers for the sparsest patterns. Given that the patterns are symmetric, there is no systematic tilting of the features. The trend of more statistical distortion and random tilting with dense patterns agrees with experiments.[6]

D. Mobility of charges in the polymer

All of the materials in this simulation (e.g., photoresist, SiO_2, and polymer) are nominally dielectrics. As a result, we assumed that there was a negligible mobility for charges for transport on and through these materials in the simulation. In measurements by Shimmura *et al.*,[5,31] evidence was found for fluorocarbon polymer having some conductivity during plasma conditions similar to those in HAR contact etching. In their experiments, polymer was deposited in a SiO_2 contact hole having a p-Si (polysilicon) bottom. Measurements of contact potentials indicated charge dissipation through the polymer to the conductive p-Si below. The mobility of charges in bulk PTFE (polytetrafluoroethylene, a first order model for the fluorocarbon polymer in features) has values of 10^{-11}–10^{-9} cm^2/V s, which would produce negligible dissipation of charge.[32,33] The experimentally observed conductivities of the polymer then resulted from, for example, energetic particle bombardment (e.g., ions and VUV photons) or nonbulk properties of the film.

In our simulations, there are no conducting materials in contact with the polymer, as in the experiments by Shimmura *et al.*[5,31] As a result, any mobility of charges in the polymer would not conduct away charge out of the feature. There could, however, be redistribution of charge within the feature. To investigate this possibility, we performed computational experiments of etching of two-dimensional (2D) trenches using the same plasma conditions as for the base case. Mobilities were specified for charge motion on and through the polymer. The values of mobilities investigated were from zero to as high as 50 cm^2/V s for both positive and negative charges. A mobility of 50 cm^2/V s is more than 10^9 times larger than found in bulk PTFE. The results of the simulation showed a negligible effect of charge mobility in the polymer on the distribution of charges and electric potentials unless the mobility has values of as large as 1–10 cm^2/V s. For example, the electric potential and charge distribution in the 2D feature are shown in Fig. 9 for having no mobility of charges in the polymer and having mobilities of 50 cm^2/V s for both positive and negative charges. Due to redistribution of the charge in the polymer and some recombination between positive and negative charges in the polymer, there is a reduction in the maximum electric potential from 585 to 501 V with mobilities of 50 cm^2/V s. However, these values of mobility are many orders of magnitude larger than those for bulk PTFE. There were no significant changes in the etch profile.

Given the large value of mobilities in the polymer required to produce significant changes in charge distribution and potential, the consequences of there being mildly conductive polymer for our simulation conditions are likely not to be large. However, the issue of conductivity of polymer in HAR etching is extremely relevant, particularly for feature architectures that have conducting materials where charge dissipation away from the feature through those

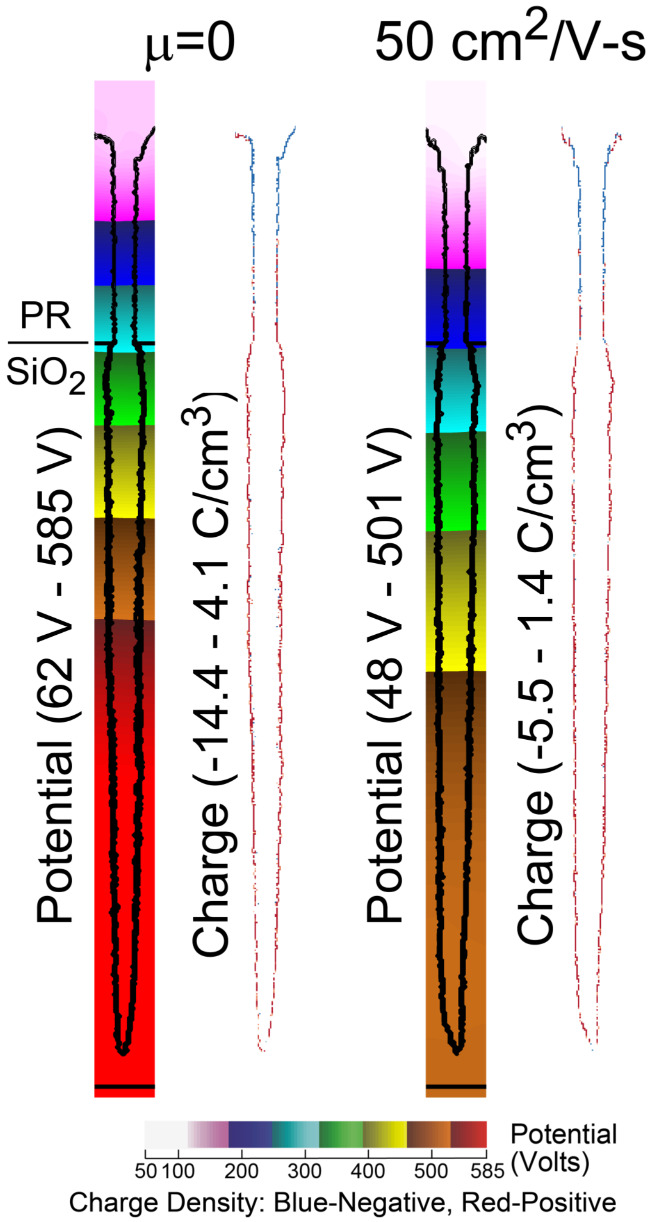

FIG. 9. Consequences of charge mobility, μ, through the polymer on electric potential and charge distributions for etching of a 2D trench in SiO_2 for the base case conditions. Potential and charge density for (left) $\mu = 0$ and (right) $\mu = 50\ cm^2/V\ s$. The electric potential is plotted with color contours. The charge density along the inside of the feature is color coded blue for negative and red for positive. The ranges of potential and charge density are noted by each image.

conductive materials can occur. The observations by Shimmura *et al.*[31] that polymer conductivity depends on the structure of the polymer is particularly relevant, as the structure is a sensitive function of the fluorocarbon gas mixtures used.

IV. CONCLUDING REMARKS

The etching of multiple HAR vias in different patterns (array, off-axis, and square) by TF-CCPs sustained in $Ar/C_4F_8/O_2$ mixtures was investigated using integrated reactor and feature scale modeling. In general, the feature-to-feature variations in etch rates and profiles mainly result from the randomness of the fluxes into adjacent features when the CDs decrease to a few tens of nanometers. The randomness is enhanced in deeper features due to the conduction limit of the incident natural radicals and roughening of sidewalls, both of which produce more statistical and smaller fluxes deep into HAR features. By allowing for some significant over-etch, the severity of randomness on feature distortion can be mitigated but at the cost of introducing systematic distortion such as additional bowing.

One cause of pattern dependent distortion in dielectric etching is perturbation of ion trajectories by the electric fields produced by charging in adjacent features. This perturbation of ion trajectories produces tilting. For features having symmetric patterns, the tilting tends to be random but not systematic. That is, the average location of the centroids of features at the stopping layer (here, at AR = 40) is generally directly under the opening in the PR. With symmetric patterns, the electric fields in a given feature produced by charging in adjacent features are, on the average, balanced by the electric fields produced by adjacent features on the opposite side.

With asymmetric patterns, the electric field due to charging in adjacent features is skewed to point from more dense to less dense areas of the pattern. That is, there is a net electric field that points from the dense regions of the pattern that are charged, on the average, more positively per unit area toward less dense regions of the pattern that are charged, on the average, less positively. The trajectories of ions are then deviated by the net horizontal electric field pointing toward the less dense pattern, producing (on the average) a systematic tilt in features toward the less dense pattern. The closer the proximity of a feature to the less dense pattern (e.g., adjacent to a vacancy in the pattern or at the edge of a pattern), the worse the systematic tilt. By increasing bias power, the energy of ions into the feature increases while the etch time decreases, resulting in some mitigation of the systematic tilting.

Simply because a region of the pattern is positively charged does not immediately imply an outward pointing tilt. It is the direction of the electric field in the features that is the important parameter. For example, if a region of the pattern is charged less positively than another region, the electric field will point toward the less positively charged region, which locally appears negatively charged, producing an inward pointing tilt. Although in feature charging is typically positive, the tops of features can be negatively charged, producing tilting or broadening of shallow features for ions having moderate energies. The more energetic the electrons that charge the top of the features, the larger the negative potential will be, extending the range of ion energies that are affected.

ACKNOWLEDGMENTS

This work was supported by the Samsung Electronics Co. Ltd. This material is also based upon work supported by the U.S. Department of Energy (DOE), Office of Science, Office of Fusion

Energy Sciences General Plasma Science Program under Award Nos. DE-SC0001319, DE-SC0014132, and DE-SC0020232. The author M.J.K. thanks Richard van Haren for discussions on sources of distortion.

REFERENCES

[1]D. J. Economou, J. Phys. D Appl. Phys. **47**, 303001 (2014).
[2]C. G. N. Lee, K. J. Kanarik, and R. A. Gottscho, J. Phys. D Appl. Phys. **47**, 273001 (2014).
[3]V. M. Donnelly and A. Kornblit, J. Vac. Sci. Technol. A **31**, 050825 (2013).
[4]M. Wang and M. J. Kushner, J. Appl. Phys. **107**, 023309 (2010).
[5]T. Shimmura, Y. Suzuki, S. Soda, S. Samukawa, M. Koyanagi, and K. Hane, J. Vac. Sci. Technol. A **22**, 433 (2004).
[6]N. Negishi, M. Miyake, K. Yokogawa, M. Oyama, T. Kanekiyo, and M. Izawa, J. Vac. Sci. Technol. B **35**, 051205 (2017).
[7]J. K. Kim, S. H. Lee, S. I. Cho, and G. Y. Yeom, J. Vac. Sci. Technol. A **33**, 021303 (2015).
[8]Y. Kim, S. Lee, T. Jung, B. Lee, N. Kwak, and S. Park, Proc. SPIE **9428**, 942806 (2015).
[9]Y. Feurprier *et al.*, Prof. SPIE **9428**, 94280F (2015).
[10]J. W. Coburn and H. F. Winters, Appl. Phys. Lett. **55**, 2730 (1989).
[11]C. Huard, Y. Zhang, S. Sriraman, A. Paterson, and M. J. Kushner, J. Vac. Sci. Technol. A **35**, 05C301 (2017).
[12]G. S. Hwang and K. P. Giapis, Phys. Rev. Lett. **79**, 845 (1997).
[13]H. W. Cheong, W. H. Lee, J. W. Kim, W. S. Kim, and K. W. Whang, Plasma Sources Sci. Technol. **23**, 065051 (2014).
[14]S.-W. Cho, J.-H. Kim, S. Kim, E. W. Shim, and C.-K. Kim, ECS J. Solid State Sci. Technol. **4**, P226 (2015).
[15]T. Tandou, S. Kubo, K. Yokogawa, N. Negishi, and M. Izawa, Precis. Eng. **44**, 87 (2016).
[16]T. Iwase, M. Matsui, K. Yokogawa, T. Arase, and M. Mori, Jpn. J. Appl. Phys. **55**, 06HB02 (2016).
[17]Y. Ban, Y. Ma, H. J. Levinson, and D. Z. Pan, J. Micro/Nanolithorg. MEMS MOEMS **9**, 041211 (2010).
[18]V. Constantoudis, V.-K. M. Kuppuswamy, and E. Gogolides, J. Micro/Nanolithorg. MEMS MOEMS **12**, 013005 (2013).
[19]N. Kuboi, T. Tatsumi, S. Kobayasgi, T. Kinoshita, J. Komachi, M. Fukasawa, and H. Ansai, Appl. Phys. Express **5**, 126201 (2012).
[20]N. Kuboi, M. Fukasawa, and T. Tatsumi, Jpn. J. Appl. Phys. **55**, 07LA02 (2016).
[21]G. Kokkoris, V. Constantoudis, P. Angelikopoulos, G. Boulousis, and E. Gogolides, Phys. Rev. B **76**, 193405 (2007).
[22]M. J. Kushner, J. Phys. D Appl. Phys. **42**, 194013 (2009).
[23]S. Huang, C. Huard, S. Shim, S. K. Nam, I.-C. Song, S. Lu, and M. J. Kushner, J. Vac. Sci. Technol. A **37**, 031304 (2019).
[24]C. Huard, Y. Zhang, S. Sriraman, A. Paterson, K. J. Kanarik, and M. J. Kushner, J. Vac. Sci. Technol. A **35**, 031306 (2017).
[25]S.-M. Kim, S. Koo, J.-T. Park, C.-M. Lim, M. Kim, C.-N. Ahn, A. Fumar-Pici, and A. C. Chen, Proc. SPIE **9048**, 90480A (2014).
[26]K. Ishikawa, K. Karahashi, T. Ishijima, S. I. Cho, S. Elliott, D. Hausmann, D. Mocuta, A. Wilson, and K. Kinoshita, Jpn. J. Appl. Phys. **57**, 06JA01 (2018).
[27]H. Ohtake, B. Jinnai, Y. Suzuki, S. Soda, T. Shimmura, and S. Samukawa, J. Vac. Sci. Technol. A **24**, 2172 (2006).
[28]V.-K. M. Kuppuswamy, V. Constantoudis, E. Gogolides, A. V. Pret, and R. Gronheid, J. Micro/Nanolithogr. MEMS MOEMS **12**, 023003 (2013).
[29]P. Nowakowski, M. Ray, P. Fischione and J. Sagar, *28th Annual SEMI Advanced Semiconductor Manufacturing Conference (ASMC)* (Saratoga Springs, New York, 2017), pp. 95–101.
[30]M. Lim, C.-M. Lim, C.-N. Ahn, D. Park, A. Fumar-Pici, and N. Seong, Proc. SPIE **10583**, 105830X (2018).
[31]T. Shimmura, S. Soda, M. Koyanagi, K. Hane, and S. Samukawa, J. Vac. Sci. Technol. B **22**, 533 (2004).
[32]M. Sessler and J. E. West, J. Appl. Phys. **47**, 3480 (1976).
[33]R. A. Moreno and B. Gross, J. Appl. Phys. **47**, 3397 (1976).